Geostrophic Adjustment for Reversibly Staggered Grids

JOHN L. MCGREGOR

CSIRO Atmospheric Research, Aspendale, Victoria, Australia

(Manuscript received 6 November 2003, in final form 28 September 2004)

ABSTRACT

A technique is presented for meteorological modeling in which all variables are held on an unstaggered grid, but the winds are transformed to a staggered C grid for the gravity wave calculations. An important feature is the use of a new reversible interpolation procedure for the staggering–unstaggering of the winds. This reversible procedure has excellent dispersion properties for geostrophic adjustment of the linearized shallow-water equations, being generally superior to those of the A, B, and C grids. Its dispersion behavior is generally similar to that of the unstaggered Z grid of Randall, which carries divergence and vorticity as primary variables. The scheme has fewer computational overheads than the Z grid.

1. Introduction

In meteorological modeling, there are several common grid arrangements for horizontally staggering the wind components relative to the mass variables. The various grids produce different behavior for geostrophic adjustment, as first clarified by Winninghoff (1968). A summary of his work, as well as a nomenclature for these common meteorological grids, was provided by Arakawa and Lamb (1977). The staggered C grid is rather popular for atmospheric models. The main reason for its popularity is that it has good dispersion behavior for large Rossby radius of deformation (defined relative to the grid spacing).

However, for small radius of deformation the C grid has poor dispersion behavior, which has resulted in greater popularity of the B grid for ocean models (e.g., Randall 1994). Randall (1994) went on to advocate the Z grid where divergence and vorticity are the primary variables, both stored on an unstaggered grid. He showed that this arrangement has superior dispersion properties for both large and small Rossby radii of deformation. The reversible staggering arrangement proposed in this paper is denoted as the R grid; it is based on the wind components but produces dispersion behavior that is generally very similar to that of the Z grid.

Unstaggered grids are appealing in that they allow the various physical parameterizations to be carried out at coincident points. An additional appeal for semi-Lagrangian models is that one set of trajectories can be used to provide common departure points for all variables. Unfortunately, the simple unstaggered A grid has quite poor dispersion properties. It also decouples into four separate families of solutions for the gravity waves (e.g., McGregor and Leslie 1977) and therefore usually requires horizontal filtering of the solutions. This decoupling problem does not occur with the staggered C grid, but it does occur to a lesser extent for the B grid. The R grid does not experience this decoupling of solutions.

Consider a formulation of the primitive equations in which all primary variables are stored on the A grid, with all physical processes and advection calculated on the A grid, but with a transformation made to the C grid for calculation of the gravity wave terms. If this staggering is done by a simple linear averaging of the wind components, the overall scheme still has the same dispersion behavior as the usual A-grid scheme, as discussed later in section 6. Higher-order interpolation may be used for the staggering–unstaggering applications, but the gravity wave dispersion characteristics remain similar to those of the A grid, as demonstrated in section 6. On the other hand, the reversible staggering procedure presented in this paper as the R-grid scheme maintains the convenience of the A grid during most calculations, but produces superior gravity wave dispersion characteristics.

The reversible staggering approach is most accurately performed in a cyclic domain. A particularly suitable grid for this purpose is the conformal-cubic grid, devised by Rancic et al. (1996); any grid line has cyclic behavior as it is followed around four panels of the cube geometry. The practicality of this grid for semi-Lagrangian advection has been demonstrated by McGregor (1996).

Corresponding author address: Dr. John L. McGregor, CSIRO Atmospheric Research, PB1 Aspendale, Vic. 3001, Australia.
E-mail: John.McGregor@csiro.au

Section 2 provides the basic equations for the reversible staggering schemes. Section 3 describes numerical evaluation of the schemes and gives examples of their interpolatory behavior. Section 4 derives the dispersion properties of the schemes for the linearized shallow-water equations. Section 5 discusses the asymmetric responses that may occur for small radii of deformation and describes a simple method to remove those asymmetries. Section 6 shows the behavior of a higher-order nonreversible scheme. Section 7 provides concluding comments.

2. Reversible staggering

The new reversible interpolation schemes are derived by considering interpolation to the "pivot" points illustrated in Fig. 1. The unstaggered x velocity components are denoted by U_m, and the staggered components by $u_{m+1/2}$. Equating the representations of U and u at the "pivot" point $x_{m+3/4}$ gives for the "left" transformation to u (or the "right" transformation back to U) the following spatially implicit "compact" formulas for the common interpolated velocity component at $x_{m+3/4}$:

- Two-point formula

$$\frac{3u_{m+1/2} + u_{m+3/2}}{4} = \frac{U_m + 3U_{m+1}}{4} \tag{1}$$

- Three-point formula

$$\frac{u_{m-1/2} + 10u_{m+1/2} + 5u_{m+3/2}}{16} = \frac{5U_m + 10U_{m+1} + U_{m+2}}{16} \tag{2}$$

- Four-point formula

$$\frac{7u_{m-1/2} + 35u_{m+1/2} + 21u_{m+3/2} + u_{m+5/2}}{64} = \frac{U_{m-1} + 21U_m + 35U_{m+1} + 7U_{m+2}}{64} \tag{3}$$

These new interpolation formulas have been derived by the generalized Vandermonde method. As may be verified by substitution, they are designed to produce a common value at the pivot points for polynomials up to order 2, 4, and 6, respectively, although the common value only exactly fits a zero- or first-order polynomial. Using symmetry, one can easily write analogous formulas for the alternative "right" transformation, based on the "pivot" point $x_{m+1/4}$.

One may instead use Lagrange interpolation, in which case (1) is unchanged, while the left-hand-side coefficients of (2) and (3) are replaced by $(-3, 30, 5)/32$ and $(-7, 105, 35, -5)/128$; the right-hand-size coefficients are replaced by $(5, 30, -3)/32$ and $(-5, 35, 105, -7)/128$, respectively. Although the Lagrange interpolation formulas produce a common value at the pivot points, they only exactly fit polynomials up to order 1, 2, and 3, respectively. It is demonstrated below that the Lagrange three-point and four-point formulas are not as accurate as (1b) and (1c) for individual Fourier components. The author is grateful to Dr. R. J. Purser of the National Centers for Environmental Prediction for suggesting use of the generalized Vandermonde method instead of Lagrange interpolation; methods for deriving related compact schemes are presented by Purser (1999).

Although it is intended that the staggering interpolation formulas (1) to (3) will be used for real variables in meteorological applications, they can also be applied to complex variables. It is instructive to consider the case of a unit-amplitude Fourier component with $U = e^{ix\theta/d}$, where d denotes the grid spacing, the wavelength is Md, and $\theta = 2\pi/M$. If the unstaggered grid points are located at $x = md$, then $U_m = e^{im\theta}$. It can be verified by substitution into (2), for example, that the corresponding staggered variables satisfy

$$u_{m+1/2} = e^{i(m+1)\theta}\frac{(e^{i\theta} + 10 + 5e^{-i\theta})}{(e^{-i\theta} + 10 + 5e^{i\theta})} \equiv e^{i(m+1/2)\theta}e^{i\phi(\theta)} \text{ say;} \tag{4}$$

a similar expression arises if (1) or (3) is used. Because the denominator of (4) is the complex conjugate of the numerator, $u_{m+1/2}$ must also have unit magnitude. This establishes the important property that the Fourier components are transformed unchanged in amplitude, undergoing only a phase shift. The expression $\phi(\theta)$ in (4) gives the phase shift of each Fourier component. For the "left" transformation schemes (1) and (3), ϕ is always positive, corresponding to a (usually small) leftward displacement.

Figure 2 plots the transformation of unstaggered unit-amplitude waves to the staggered grid, as evaluated from the real part of (4), or from versions of (4) modified for the other interpolation formulas. There is a large phase lag for two-grid waves, a small lag for

FIG. 1. Relative location of unstaggered (|) and staggered (×) grid points, and "pivot" points (★).

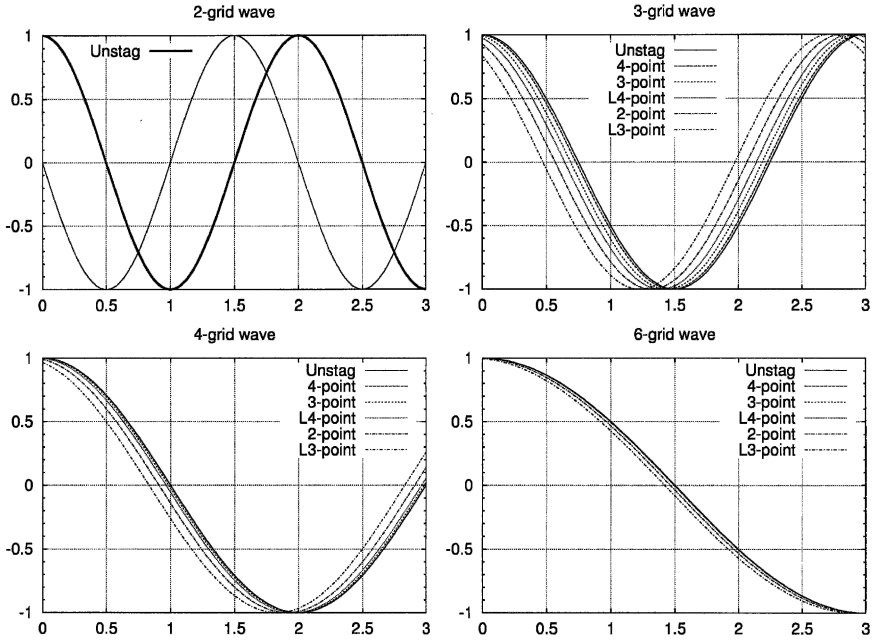

FIG. 2. Unstaggered (thick line) and staggered representations of (a) two-, (b) three-, (c) four-, and (d) six-grid waves. The staggered representations for the various schemes are shown for two-, three-, and four-point schemes and for Lagrange three- and four-point schemes; the captions are listed in decreasing order of accuracy. All schemes produce identical results for two-grid waves, being a displacement of the staggered pattern by 0.5 grid points to the left. The horizontal axis is in units of grid lengths.

three-grid waves, and even smaller lags for the higher waves. It is readily shown that the root-mean-square difference between the unstaggered and staggered fields is given by $(1 - \cos\phi)^{1/2}$. This behavior is quantified in Table 1, which gives the root-mean-square differences and lags between the unstaggered and staggered families. The smallest differences are found for the three- and four-point Vandermonde schemes. For all schemes, the differences reduce for the better-resolved waves.

It should be noted that faithful representation of two-grid waves can never be achieved, and three-grid waves cannot be well resolved numerically. McDonald (1984) illustrates this for advection, using a cubic semi-Lagrangian scheme, finding for a Courant number of 0.25 that unit-amplitude waves will have their amplitude reduced after one advective time step to 0.56, 0.80, 0.92, 0.96, and 0.98, respectively, for two-, three-, four-, five-, and six-grid waves, while their phase velocities will be 0%, 78%, 93%, 97%, and 98% of the true value. An important property of the present schemes is that even two-grid or three-grid features can be maintained, without any extra damping from the staggering–unstaggering process.

3. Numerical evaluation of the staggering transformations

Each of the staggering–unstaggering Eqs. (1)–(3) forms a linear system that may be solved as a matrix inversion problem. For the two-, three- and four-point schemes, respectively, the dominant terms (for a periodic domain) are

$$u_{m+1/2} = 0.33U_m + 0.89U_{m+1} - 0.30U_{m+2} + 0.10U_{m+3} - 0.03U_{m+4} + 0.01U_{m+5}, \quad (5)$$

TABLE 1. Root-mean-square differences between the unstaggered and staggered representations of unit two-, three-, four-, and six-grid waves for the three reversible Vandermonde schemes, as well as the reversible Lagrange (L3 and L4) schemes. The phase lag is shown in parentheses (in units of grid length). The schemes are listed in decreasing order of accuracy.

	Two-grid wave	Three-grid wave	Four-grid wave	Six-grid wave
Four-point scheme	1.000 (0.5)	0.030 (0.02)	0.003 (0.00)	0.000 (0.00)
Three-point scheme	1.000 (0.5)	0.091 (0.06)	0.017 (0.02)	0.002 (0.00)
L4 scheme	1.000 (0.5)	0.159 (0.11)	0.040 (0.04)	0.006 (0.01)
Two-point scheme	1.000 (0.5)	0.267 (0.18)	0.100 (0.09)	0.027 (0.04)
L3 scheme	1.000 (0.5)	0.403 (0.28)	0.186 (0.17)	0.059 (0.08)

$$u_{m+1/2} = 0.03U_{m-1} + 0.26U_m + 0.93U_{m+1} - 0.25U_{m+2} + 0.04U_{m+3} - 0.01U_{m+4}, \quad (6)$$

$$u_{m+1/2} = -0.02U_{m-1} + 0.40U_m + 0.85U_{m+1} - 0.32U_{m+2} + 0.14U_{m+3} - 0.06U_{m+4} + 0.03U_{m+5} - 0.01U_{m+6}. \quad (7)$$

While these expressions are useful for illustrating the nature of the solutions, they converge too slowly to be recommended. Accurate and efficient evaluation may be obtained by use of a tridiagonal solver for the two- and three-point schemes. The periodic nature of the conformal-cubic grid requires a cyclic tridiagonal solver, such as that described by Temperton (1975). To apply the four-point formulas, a pentadiagonal solver may be used such as the cyclic scheme described by Navon (1987).

Alternatively, it is straightforward to devise iterative solutions to (1)–(3). An efficient solution follows for the three-point scheme (2). First, the equation is combined with itself to bring out a diagonal dominance; multiplying (2) by 32 and subtracting 16 times (2) evaluated for $m + 1$ gives

$$2u_{m-1/2} + 19u_{m+1/2} - 5u_{m+5/2} = 10U_m + 15U_{m+1} - 8U_{m+2} - U_{m+3}. \quad (8)$$

Given values for the unstaggered U, (8) suggests the following iterative solution:

first guess:

$$u^0_{m+1/2} = (10U_m + 15U_{m+1} - 8U_{m+2} - U_{m+3})/19; \quad (9)$$

later iterations:

$$u^n_{m+1/2} = u^0_{m+1/2} - \frac{2u^{n-1}_{m-1/2}}{19} + \frac{5u^{n-1}_{m+5/2}}{19}. \quad (10)$$

Four iterations are found to give good convergence. The corresponding formulas for unstaggering may be written in the obvious manner.

4. Dispersion behavior for the shallow-water equations

Adopting the notation of Arakawa and Lamb (1977), the shallow-water equations linearized about a resting basic state are written as

$$\frac{\partial u}{\partial t} - fv + g\frac{\partial h}{\partial x} = 0, \quad (11)$$

$$\frac{\partial v}{\partial t} + fu + g\frac{\partial h}{\partial y} = 0, \quad (12)$$

$$\frac{\partial h}{\partial t} + H\left(\frac{\partial u}{\partial x} + \frac{\partial v}{\partial y}\right) = 0, \quad (13)$$

where H is the constant depth of the "water" in the basic state, f is the constant Coriolis parameter on the f plane, and all other symbols have their conventional meanings. Wave solutions of the form

$$u = Ae^{i(kx+ly+\sigma t)}, v = Be^{i(kx+ly+\sigma t)}, h = Ce^{i(kx+ly+\sigma t)} \quad (14)$$

are now substituted for u, v, and h. As noted by Randall (1994), the continuous equations produce the dispersion relation

$$\left(\frac{\sigma}{f}\right)^2 = 1 + \lambda^2(k^2 + l^2). \quad (15)$$

Here σ is the frequency, $\lambda = (gH)^{1/2}/f$ is the radius of deformation, and k and l are wavenumbers in the x and y directions, respectively.

An analysis is presented here for schemes where all the variables are stored at unstaggered A-grid positions, but the wind components are transformed to the staggered C-grid positions for the gravity wave calculations. Equations (11)–(13) are treated in the following manner. The horizontal height derivatives in (11) and (12) are calculated at the staggered positions, using the simplest centered two-point formula, then those derivatives are transformed to the unstaggered positions [this strategy for treating the height derivatives has been found to be very beneficial in the semi-Lagrangian Commonwealth Scientific and Industrial Research Organisation (CSIRO) conformal-cubic climate model, as it allows a subsequent consistent semi-implicit derivation of the heights in that model]. The Coriolis terms are evaluated at the unstaggered positions. The divergence in (13) is evaluated at unstaggered locations by using centered two-point differences of the velocity components u and v, which have been transformed to the staggered locations. The analysis is designed to cover the present reversible scheme, as well as simpler averaging schemes.

The exponential wave solutions for u, v, and h are all taken as being defined exactly at the unstaggered (x, y) positions, for a grid spacing d. For a transformation half a grid length to the staggered positions, the x Fourier component is multiplied by $\zeta(kd/2)$, say. The reverse transformation from staggered to unstaggered positions multiplies the Fourier component by $\zeta'(kd/2)$, say. In the notation of (4), ζ and ζ' may be written as

$$\zeta\left(\frac{kd}{2}\right) = e^{i\phi(kd)}, \zeta'\left(\frac{kd}{2}\right) = e^{-i\phi(kd)}. \quad (16)$$

Making the appropriate Fourier substitutions (14) into (11)–(13) and dividing by the common factor $e^{i(kx+ly+\sigma t)}$ yields, respectively,

$$i\sigma A - fB + C\frac{2ig}{d}\zeta'\left(\frac{kd}{2}\right)\sin\frac{kd}{2} = 0, \tag{17}$$

$$i\sigma B + fA + C\frac{2ig}{d}\zeta'\left(\frac{ld}{2}\right)\sin\frac{ld}{2} = 0, \tag{18}$$

$$i\sigma C + \frac{2iH}{d}\left\{A\zeta\left(\frac{kd}{2}\right)\sin\frac{kd}{2} + B\zeta\left(\frac{ld}{2}\right)\sin\frac{ld}{2}\right\} = 0. \tag{19}$$

Substituting C from (19) into (17) and (18), respectively, gives

$$A\left\{i\sigma - \frac{4iHg}{\sigma d^2}\zeta\left(\frac{kd}{2}\right)\zeta'\left(\frac{kd}{2}\right)\sin^2\frac{kd}{2}\right\} = B\left\{f + \frac{4iHg}{\sigma d^2}\zeta'\left(\frac{kd}{2}\right)\zeta\left(\frac{ld}{2}\right)\sin\frac{kd}{2}\sin\frac{ld}{2}\right\}, \tag{20}$$

$$A\left\{f - \frac{4iHg}{\sigma d^2}\zeta\left(\frac{kd}{2}\right)\zeta'\left(\frac{ld}{2}\right)\sin\frac{kd}{2}\sin\frac{ld}{2}\right\} = -B\left\{i\sigma - \frac{4iHg}{\sigma d^2}\zeta\left(\frac{ld}{2}\right)\zeta'\left(\frac{ld}{2}\right)\sin^2\frac{ld}{2}\right\}. \tag{21}$$

The dispersion equation for σ/f follows from (20) and (21) as

$$\left(\frac{\sigma}{f}\right)^2 = 1 + \frac{4\lambda^2}{d^2}\left\{\zeta\left(\frac{kd}{2}\right)\zeta'\left(\frac{kd}{2}\right)\sin^2\frac{kd}{2} + \zeta\left(\frac{ld}{2}\right)\zeta'\left(\frac{ld}{2}\right)\sin^2\frac{ld}{2}\right\} + \frac{4i\lambda^2}{d^2}\frac{f}{\sigma}\left\{\zeta'\left(\frac{kd}{2}\right)\zeta\left(\frac{ld}{2}\right) - \zeta\left(\frac{kd}{2}\right)\zeta'\left(\frac{ld}{2}\right)\right\}\sin\frac{kd}{2}\sin\frac{ld}{2}, \tag{22}$$

where the radius of deformation, λ, has been substituted. For the reversible schemes $\zeta(kd/2)\zeta'(kd/2) = 1$, so that substitution of (16) into (22) gives the dispersion formula

$$\left(\frac{\sigma}{f}\right)^2 = 1 + \frac{4\lambda^2}{d^2}\left\{\sin^2\frac{kd}{2} + \sin^2\frac{ld}{2}\right\} + \frac{8\lambda^2}{d^2}\frac{f}{\sigma}\sin[\phi(kd) - \phi(ld)]\sin\frac{kd}{2}\sin\frac{ld}{2}, \tag{23}$$

where all the imaginary terms have vanished.

The final term introduces an asymmetry for the x and y responses; its magnitude is small compared to the sum of the other two terms, so that σ/f is readily evaluated by simple iteration. Apart from this small asymmetric term, the dispersion equation is identical to that given by Randall (1994) for his Z grid, where vorticity and divergence were used as the primary variables.

Figure 3 shows the dispersion behavior for the continuous equations and for the A, B, C, R, and Z grids, for a typical atmospheric radius of deformation, $\lambda/d = 2$. The R grid plots are for the three-point scheme; the other dispersion plots use the formulas given by Randall (1994). The plot for the R grid scheme is very similar to those of the C and Z grids and has the same qualitative behavior as the solution to the continuous equations.

Figure 4 replots the dispersion behavior for cross sections along the edges and along a diagonal. It can be seen that the R and Z schemes are identical along the $kd = 0$, $ld = 0$, and $kd = ld$ cross sections, and both are slightly superior to the C scheme. The remaining cross sections reveal a small asymmetry for the R scheme for both the shortest x and y wavelengths, corresponding to the asymmetry noted above in the dispersion relation (23). In all the figures, a "left" transformation has been used, producing a positive ϕ in (4). From (23), the figures are then consistent with an increase in frequency when $kd > ld$ and a decrease when $kd < ld$. The two-point and four-point versions of the R-grid scheme, denoted as R2 and R4 but not plotted here, are almost identical to the three-point scheme. Cross sections are also shown for a modified A scheme, denoted by A4 and described later in section 6.

As displayed by Randall (1994), it is instructive to also show results for a typical oceanic radius of deformation, $\lambda/d = 0.1$. Figure 5 shows the corresponding dispersion behavior for the A, B, C, R, and Z grids. As noted by Randall (1994), the Z grid shows closest qualitative correspondence to the solution of the continuous equations. However, the R grid also shows commendable qualitative correspondence, appearing superior to the remaining grid types. The corresponding cross sections are shown in Fig. 6. This clarifies that the R scheme has an unphysical maximum near the two-grid y position, and an unphysical minimum near the two-grid x position. The dispersion behavior of the R2 and R4 versions are also plotted; the asymmetry is somewhat smaller with the R2 scheme, for this case of small radius of deformation. Note that the asymmetry of the R-grid schemes will be of opposite sign if a "right" transformation is used in place of the "left" transformation (1) to (3) for calculating the grid transformations.

5. Discussion and removal of the asymmetric responses

As noted in the previous section, the dispersion relation (23) displays some asymmetric responses for small wavelength features under situations having small radii of deformation. Dr. N. Wood of the U.K. Met Office (2004, personal communication) has provided some insights into the nature of the asymmetric responses. The following equations are largely based on his comments.

Equation (23) may be rewritten as a cubic equation in σ/f,

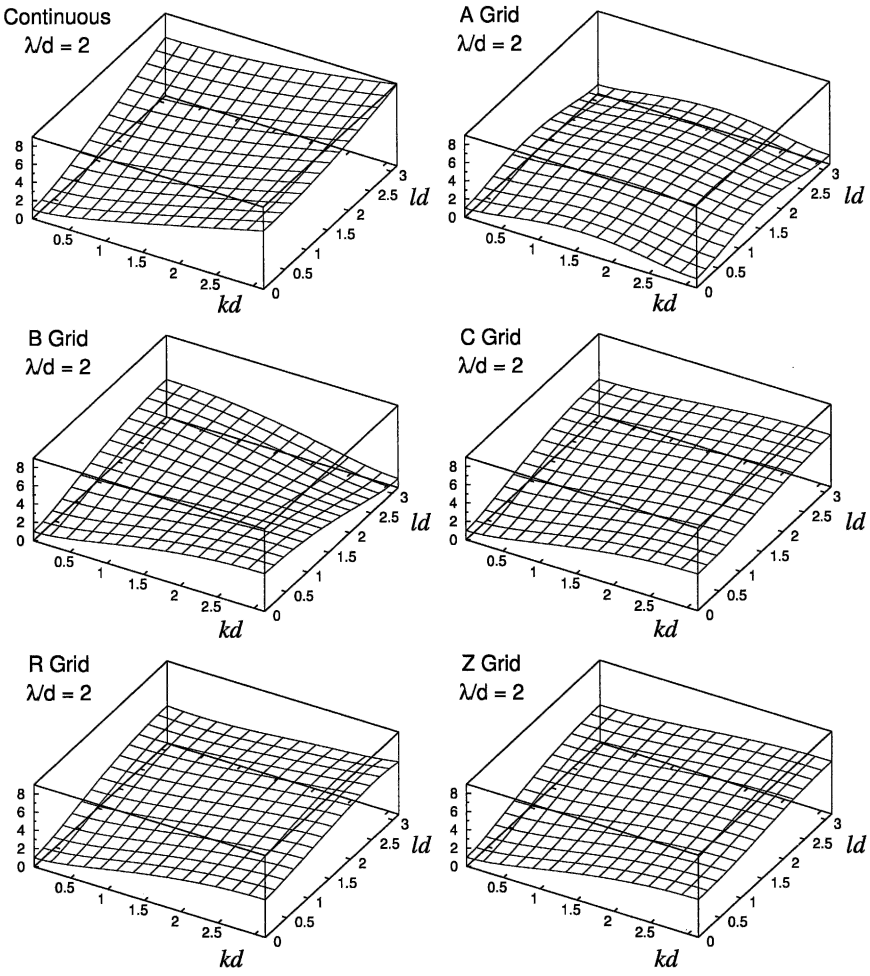

FIG. 3. Dispersion behavior for the continuous equations and for the A, B, C, R, and Z grids, for the case $\lambda/d = 2$. The vertical coordinate is the normalized frequency σ/f. The horizontal coordinates are kd and ld, respectively. Two-grid waves correspond to $kd = \pi$ and $ld = \pi$, respectively.

$$\left(\frac{\sigma}{f}\right)^3 = \frac{\sigma}{f} + \frac{4\lambda^2}{d^2}\frac{\sigma}{f}\left\{\sin^2\frac{kd}{2} + \sin^2\frac{ld}{2}\right\} + \frac{8\lambda^2}{d^2}\sin[\phi(kd) - \phi(ld)]\sin\frac{kd}{2}\sin\frac{ld}{2}. \quad (24)$$

It should be noted that the derivation of the analytical dispersion relation (15) also arises from a cubic equation in σ/f, but a root $\sigma/f = 0$ has been canceled and thereby neglected. This neglected root corresponds to the degenerate stationary Rossby mode, in the analytical case. However, in (23) no longer does a root $\sigma/f = 0$ factor out. The consequence of this is that, what in the analytical case corresponds to the stationary Rossby wave is now a spuriously propagating wave. To gain some insight into its frequency, rewrite (23) as

$$\left(\frac{\sigma}{f}\right)\left[\left(\frac{\sigma}{f}\right)^2 - a^2\right] = \varepsilon, \quad (25)$$

where

$$a^2 \equiv 1 + \frac{4\lambda^2}{d^2}\left\{\sin^2\frac{kd}{2} + \sin^2\frac{ld}{2}\right\}, \quad (26)$$

with a necessarily real, and

$$\varepsilon \equiv \frac{8\lambda^2}{d^2}\sin[\phi(kd) - \phi(ld)]\sin\frac{kd}{2}\sin\frac{ld}{2}. \quad (27)$$

When ε is small, the roots to (25) to order ε^3 are

$$\left(\frac{\sigma}{f}\right) = -\frac{\varepsilon}{a^2} + O(\varepsilon^3), \quad (28)$$

and

$$\left(\frac{\sigma}{f}\right) = \pm a + \frac{\varepsilon}{2a^2} + O(\varepsilon^3). \quad (29)$$

It may be noted that both expressions contain only

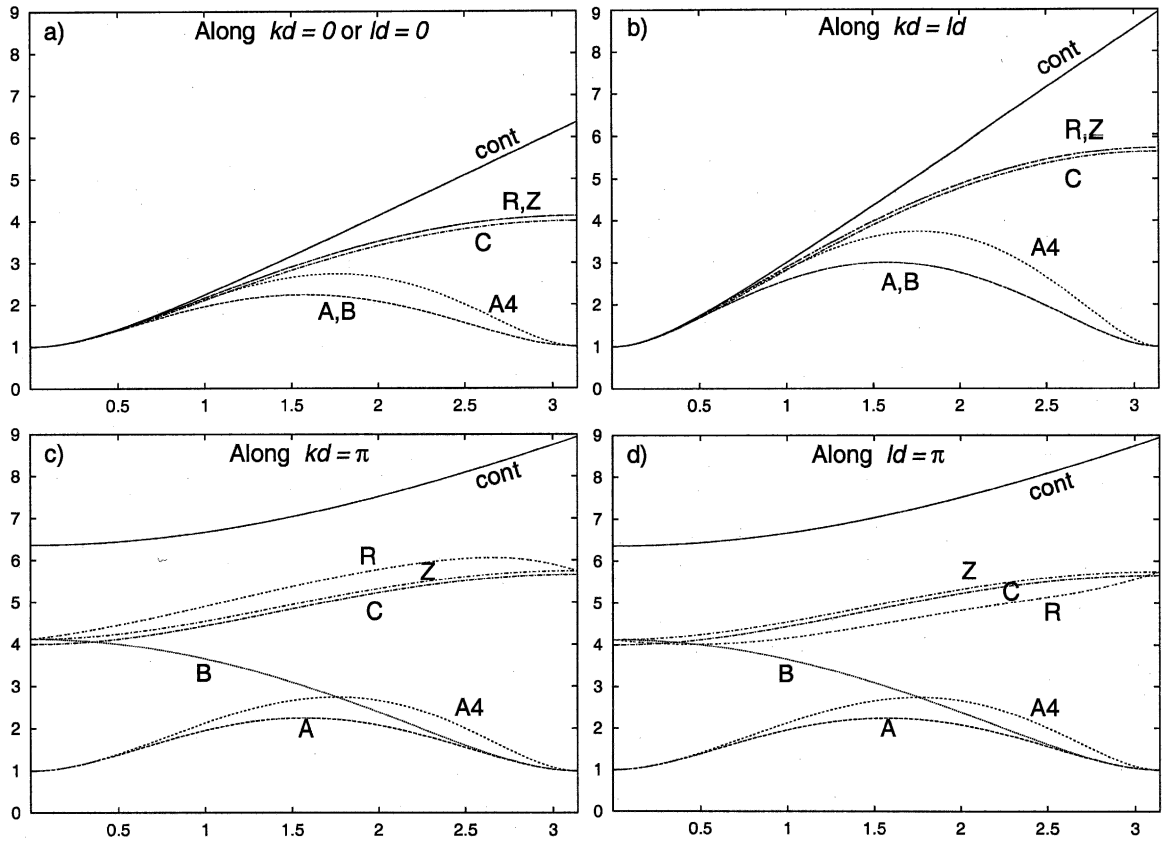

FIG. 4. Dispersion behavior for $\lambda/d = 2$ as in Fig. 3, but (a)–(d) showing four different cross sections; curves for the A4 scheme are also included.

odd powers of ε. These equations show that the analytically decoupled Rossby mode has become weakly coupled with the gravity wave modes, which could conceivably cause problems if the effect was systematic. Another problem may conceivably arise from the directional asymmetry of the propagation speeds of narrow features (those having close to a two-grid-length structure in either, but not both, of the x and y directions, as seen in Figs. 6c and 6d) for situations of small radius of deformation.

It is in fact possible to remove the asymmetry arising in the shallow-water dispersion equations. This may be achieved by alternately utilizing a "left" and "right" staggering in alternate time steps. Making the reasonable assumption that a gravity wave propagating in a certain direction during the first time step is to be associated with the gravity wave propagating with a similar speed and direction during the second time step, the frequency error in the second step cancels that of the first step, because of the reversed sign of ε appearing in (29). Thus at the end of every second step, the wave satisfies the same dispersion relationship as for the Z grid; the Rossby mode also becomes stationary. The situation is, of course, more complicated for a full primitive equations model in which advection and other physical processes also occur during each time step. However, it is to be expected that this alternating treatment will avoid the tendency for development of any systematic effects related to asymmetric dispersion responses during an individual time step. To test for systematic effects, multiple 12-month simulations at approximately 200-km resolution have been performed with the CSIRO semi-Lagrangian conformal-cubic atmospheric climate model; no significant difference in climatology has been found between simulations with either type of staggering and the alternating version. It should be noted that a tempting treatment is to apply the alternative staggering transformations during a repeated model time step and to use the average result of the two calculations; however, this treatment does not preserve the magnitude of a unit-amplitude wave, so it is not recommended.

6. Comparison to averaging schemes

For linear interpolation (two-point, denoted here as A), the transformations to and from the staggered positions are given by

$$\zeta\left(\frac{kd}{2}\right) = \zeta'\left(\frac{kd}{2}\right) = \cos\frac{kd}{2}, \tag{30}$$

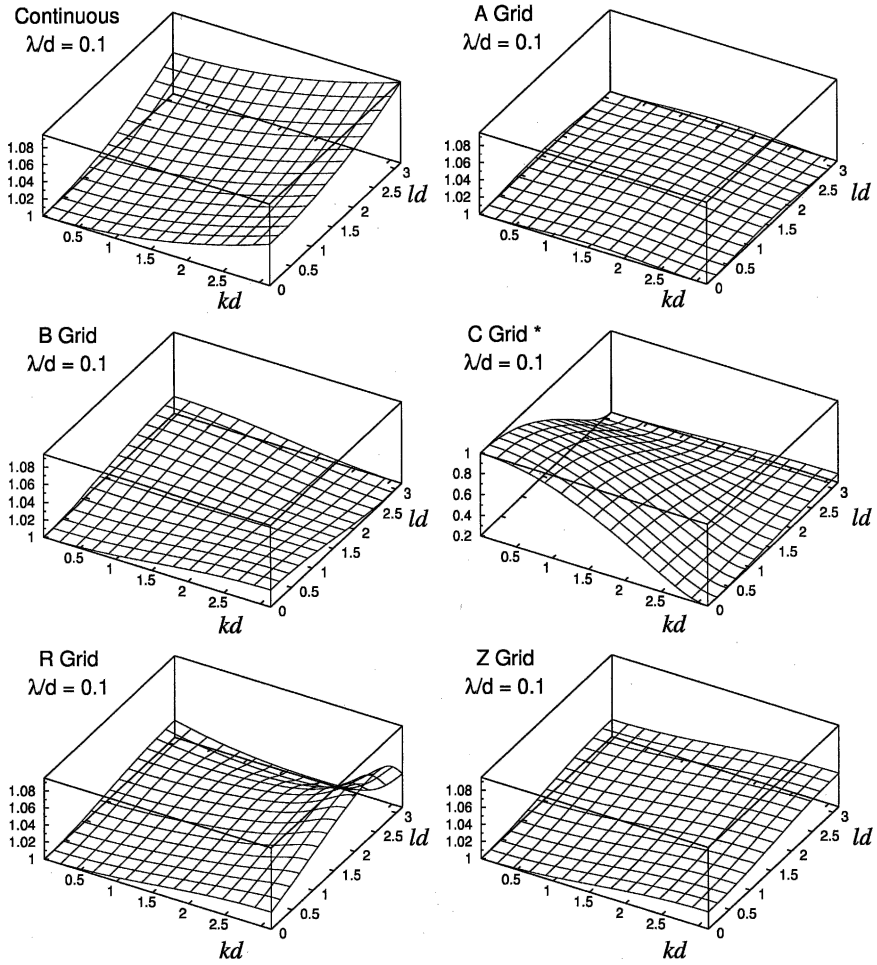

FIG. 5. Dispersion behavior for the A, B, C, R, and Z grids as in Fig. 3, but for the case $\lambda/d = 0.1$; note the different vertical scale for the C grid (*).

while for Lagrange cubic interpolation (four-point, denoted here as A4), the transformations are

$$\zeta\left(\frac{kd}{2}\right) = \zeta'\left(\frac{kd}{2}\right) = \frac{9}{8}\cos\frac{kd}{2} - \frac{1}{8}\cos\frac{3kd}{2}. \quad (31)$$

For both these cases, the final term in (22) vanishes. As might be expected, for linear interpolation the resulting dispersion Eq. (22) is identical to the A-grid formula given by Randall (1994). The cross-section plots of Figs. 4 and 6 include, respectively, the dispersion behavior for the A4 scheme for the cases $\lambda/d = 2$ and $\lambda/d = 0.1$. The A4 scheme has qualitatively very similar behavior to the linear A scheme. In fact, it can be seen that its frequencies are a little better than for the A scheme, but are still significantly inferior to those of the R and Z schemes. An advantage of the A4 grid over the A grid is that the usual decoupling of the A-grid solution into four solutions (e.g., McGregor and Leslie 1977) does not occur with the A4 grid. This can be seen by substituting horizontally differenced versions of (11) and (12) into (13), giving that each new value of h depends on a form of $\nabla^2 h$ whose definition includes eight adjacent x neighbors and eight y neighbors.

The cubic interpolation A4 approach has some similarities to the method used by Dietrich (1997). In his ocean model, he uses cubic interpolation to calculate velocities at the staggered positions. The subsequent tendencies of the staggered velocities are then reinterpolated to provide increments for the velocities at the unstaggered locations. The dispersion analysis in this paper cannot be applied to the scheme of Dietrich (1997) without modifying it to introduce a dependence on the time step. Although his interpolatory scheme is not reversible, he does claim reduced numerical dispersion.

7. Concluding comments

A new technique has been proposed for meteorological modeling in which all variables may be stored on an

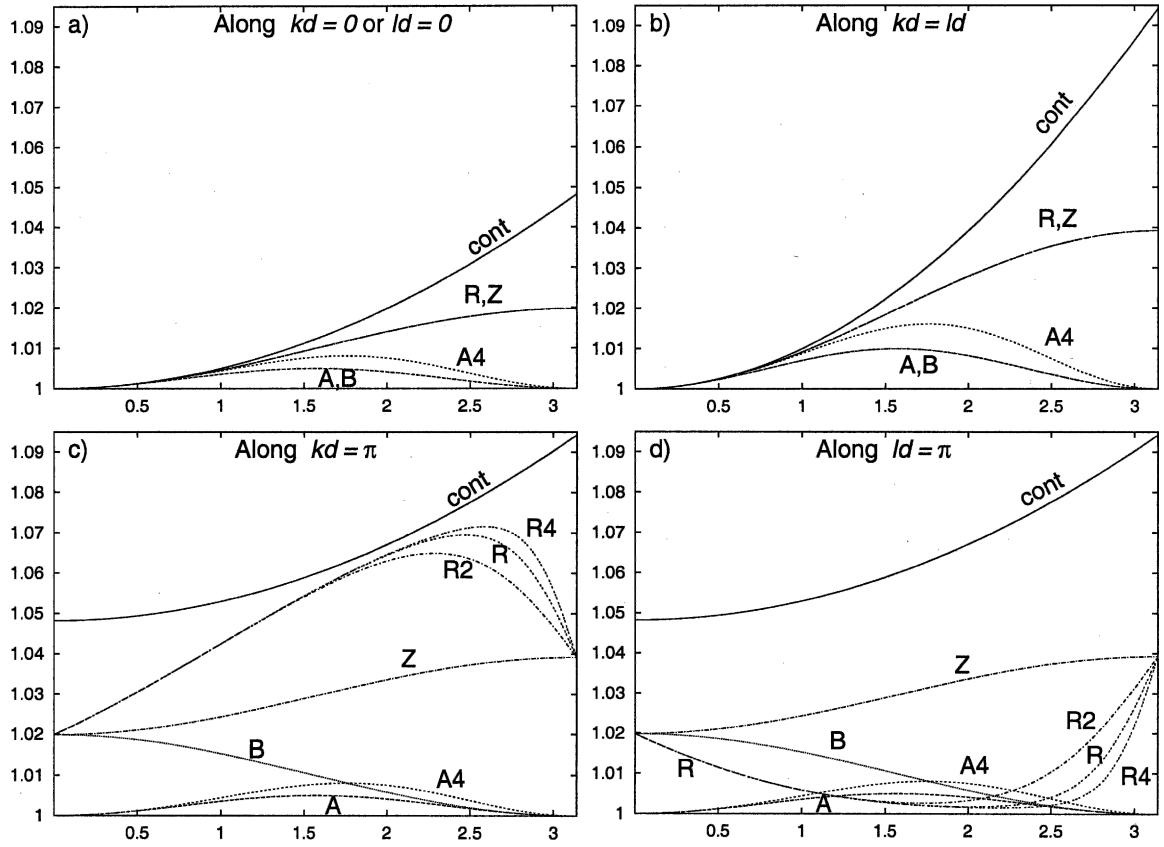

FIG. 6. Dispersion behavior for $\lambda/d = 0.1$ as in Fig. 5, but (a)–(d) showing four different cross sections; curves for the R2, R4, and A4 schemes are also included; the C-grid curve is not shown, as its frequency is always less than 1.

unstaggered grid. Unstaggered grids are advantageous for implementing physical parameterizations; they also allow simpler calculation of trajectories for semi-Lagrangian models. To achieve good geostrophic adjustment behavior, the wind components are reversibly transformed onto a staggered C grid for the gravity wave calculations. This reversible arrangement is denoted as the R grid. A "compact" definition of the reversible interpolation equations was given, and it was proved that Fourier components are not damped by the interpolations. Three separate formulas were investigated, based on two-, three-, and four-point versions of the "compact" equations. The interpolation behavior is similar for all three versions.

The R-grid schemes have excellent dispersion characteristics for geostrophic adjustment of the shallow-water equations, being similar to those of the Z-grid scheme of Randall (1994), where divergence and vorticity are carried as primary variables. The dispersion properties are generally superior to those of the more common A, B, and C grids. There is a minor x–y asymmetry near the location of two-grid waves; this asymmetry is negligible for the larger radii of deformation typical of meteorological applications, but it is discussed further in section 5. The asymmetry can be readily removed by alternating the direction of staggering from one time step to the next, in which case the dispersion properties become the same as those of the Z grid. There are fewer computational overheads for the R-grid schemes than for the Z grid, because the staggering–unstaggering consists of straightforward one-dimensional calculations, rather than requiring Laplacian inversions to diagnose the winds from the divergence and vorticity. It should be mentioned that, in the context of a hexagonal grid system, Ringler and Randall (2002) have recently devised the ZM grid system, which is based on mass points and extra staggered momentum points and which possesses the same favorable geostrophic adjustment properties as the Z grid.

An alternative nonreversible A4 staggering scheme was also investigated based on cubic interpolation. The dispersion properties of this scheme were inferior to the R-grid schemes, being essentially the same as for the original A grid. However, the A4 scheme does avoid the usual solution decoupling of the A grid.

The reversible staggering scheme has been successfully incorporated into a general circulation model formulated on the conformal-cubic grid of Rancic et al. (1996), with the semi-Lagrangian advection handled by the methods of McGregor (1993, 1996). The reversible

staggering scheme is found to work equally well for quasi-uniform and stretched-grid versions of the model. It has been found that the jet intensities are maintained much better by this reversible staggering than a previous implementation using a nonreversible cubic A4 scheme. Some preliminary results for this model are given by McGregor and Dix (2001) and McGregor et al. (2002).

As a final clarification, it should be noted that reversible schemes are not being advocated here for routine curve-fitting or surface-fitting applications; for those applications, considerations such as the order of the interpolation scheme or its shape-preserving attributes will usually be more important. The important advantages of reversible schemes will arise in solving systems of equations where certain variables are required at both staggered and unstaggered locations, and a consistent transformation to and from those locations is desired. Other possible advantageous applications of the reversible interpolation technique include vertical advection and ocean modeling; note that for those applications the method will need modifications to account for an absence of periodicity along the coordinate lines.

Acknowledgments. The author is grateful to Dr. R. J. Purser of the National Centers for Environmental Prediction for suggesting use of the generalized Vandermonde method to derive the interpolation formulas. He is also grateful to Drs. Nigel Wood, Todd Ringler, and Martin Dix for their valuable comments during the review process.

REFERENCES

Arakawa, A., and V. R. Lamb, 1977: Computational design of the basic dynamical processes of the UCLA general circulation model. *Methods Comput. Phys.,* **17,** 173–265.

Dietrich, D. E., 1997: Application of a modified Arakawa 'a' grid ocean model having reduced numerical dispersion to the Gulf of Mexico circulation. *Dyn. Atmos. Oceans,* **27,** 210–217.

McDonald, A., 1984: Accuracy of multiply-upstream, semi-Lagrangian advective schemes. *Mon. Wea. Rev.,* **112,** 1267–1275.

McGregor, J. L., 1993: Economical determination of departure points for semi-Lagrangian models. *Mon. Wea. Rev.,* **121,** 221–230.

——, 1996: Semi-Lagrangian advection on conformal-cubic grids. *Mon. Wea. Rev.,* **124,** 1311–1322.

——, and L. M. Leslie, 1977: On the selection of grids for semi-implicit schemes. *Mon. Wea. Rev.,* **105,** 236–238.

——, and M. R. Dix, 2001: The CSIRO conformal-cubic atmospheric GCM. *IUTAM Symposium on Advances in Mathematical Modelling of Atmosphere and Ocean Dynamics,* P. F. Hodnett, Ed., Kluwer, 197–202.

——, K. C. Nguyen, and J. J. Katzfey, 2002: Regional climate simulations using a stretched-grid global model. Research Activities in Atmospheric and Oceanic Modelling Rep. 32, WMO Tech Doc. 1105*,* 2 pp.

Navon, I. M., 1987: PENT: A periodic cyclic pentadiagonal system solver. *Commun. Numer. Methods,* **3,** 63–69.

Purser, R. J., 1999: Efficient high-order semi-Lagrangian methods. *Proc. Seminar on Recent Developments in Numerical Methods for Atmospheric Modelling,* Reading, United Kingdom, ECMWF, 73–94.

Rancic, M., R. J. Purser, and F. Mesinger, 1996: A global shallow-water model using an expanded spherical cube: Gnomonic versus conformal coordinates. *Quart. J. Roy. Meteor. Soc.,* **122,** 959–982.

Randall, D. A., 1994: Geostrophic adjustment and the finite-difference shallow-water equations. *Mon. Wea. Rev.,* **122,** 1371–1377.

Ringler, T. D., and D. A. Randall, 2002: The ZM grid: An alternative to the Z grid. *Mon. Wea. Rev.,* **130,** 1411–1422.

Temperton, C., 1975: Algorithms for the solution of cyclic tridiagonal systems. *J. Comput. Phys.,* **19,** 317–323.

Winninghoff, F. J., 1968: On the adjustment toward a geostrophic balance in a simple primitive equation model with application to the problems of initialization and objective analysis. Ph.D. thesis, University of California, Los Angeles, 161 pp.